Cellular and Molecular Imaging: non-proton MRI

Andrew Webb. C.J.Gorter Centre for High Field MRI,
Department of Radiology, Leiden University Medical Centre,
Albinusdreef 2, 2333 ZA Leiden, The Netherlands.
Email: a.webb@lumc.nl

Cellular and molecular imaging (CMI) can be defined broadly as the in vivo monitoring of complicated pathological processes via detection of *specific* biological signatures at the sub-cellular level. Although most CMI using magnetic resonance (MR) is performed using specialized agents that are injected into the body, endogenous molecules *intrinsic* to the body can also act as potential molecular markers of disease.

The vast majority of CMI is performed using proton-detected magnetic resonance due to the high signal-to-noise ratio (SNR), the commercial availability of a wide-range of radiofrequency coils for both human and animal work, and the simplicity of sequence implementation on the scanner. However, proton-based molecular imaging, while having high sensitivity in terms of limits-of-detection, does suffer from low *specificity*: in other words the MRI signal is dominated by the large non-specific water contribution. Although altered tissue proton relaxation times and diffusion characteristics, for example, can be sensitive measures of gross pathological conditions, the fact that these changes represents a summation of inter- and extra-cellular changes means that this type of monitoring is quite aspecific.

In contrast, heteronuclear ie non-proton detection increases the specificity of the measurements significantly. The disadvantages of heteronculear MRI are well-known: low SNR typically mean long acquisition times and/or poor spatial resolution. Table 1 shows the relative sensitivities of four different heteronuclei that have been used for molecular imaging. ^{19}F and ^{13}C represent exogenous agents that have been introduced into the body, whereas ^{31}P and ^{23}Na are endogenous.

Table 1

Element	γ relative to ^{1}H	Natural abundance	Sensitivity relative to ^{1}H	Other relevant MR characteristics
^{19}F	0.94	100%	0.83	Long T_1, long T_2 ^{1}H-^{19}F and ^{19}F-^{19}F Jcoupling Large chemical shift range Not present in body
^{31}P	0.40	100%	0.0066	Long T_1, short T_2 Small chemical shift range Millimolar concentrations
^{13}C	0.25	1.1%	0.00017	Long T_1, long T_2 Large chemical shift range Millimolar concentrations Hyperpolarized or ^{13}C enriched
^{23}Na	0.26	100%	0.093	Short T_1, Biexponential short T_2 Single peak Tens to hundreds of mM

Fluorine-19 based exogenous agents

The concept of using ^{19}F as an MR marker has many attractive features including:

(i) The highest gyromagnetic ratio next to proton (and tritium)
(ii) Very common use of radioactive ^{18}F in positron emission tomography (PET) studies
(iii) Similarity in function and structure of fluorinated moleculars to their protonated analogues
(iv) Biocompatibility of perfluorocarbons (e.g. used as blood substitutes)
(v) No backgrounds signal, resulting in high dynamic range images

With fluorine MR one can use the signal intensity directly for quantitation, rather than needing to acquire pre- and post-injection proton images (since there is no background signal in the body for fluorine), nor must one consider the indirect effect of magnetization transfer or relaxation times as mediating factors in the proton signal intensity.

The major challenge is to target a sufficient concentration of fluorine molecules to the site of interest in order to get sufficient MR signal. Most work has used some form of encapsulation of perfluorocarbons, since these compounds can be used in very high concentrations and have many fluorine atoms, albeit resonating at different frequencies. Since perfluorocarbons are highly lipophilic/hydrophobic special encapsulation technology has to be used. Non-targeted protein microspheres were initially developed [1], but "targeting" was only to macrophages in the liver and spleen.

The most recent developments have centred on site-targeted paramagnetic perfluorocarbon (PFC) nanoparticles [2-5]. These have been proposed for targeting angiogenesis since the growth of new blood vessels associated with many tumours can be targeted by considering biomarkers such as $\alpha_v\beta_3$ integrin which is exposed to the vessel lumen on activated endothelial cells, but is not expressed otherwise. Typical fluorine compounds consist of a single peak (crown ethers, can show chemical structure) but can contain many peaks (PFOB, structure). The latter has a lower SNR (unless deconvolution techniques are used for imaging) but it is known that the relative chemical shifts depend on temperature, oxygenation and pH, and so can be used as molecular imaging agents in these regards. Figure 1 shows a schematic of a PFOB-filled nanoparticle, with a quinolone nonpeptide as an $\alpha_v\beta_3$ integrin antagonist.

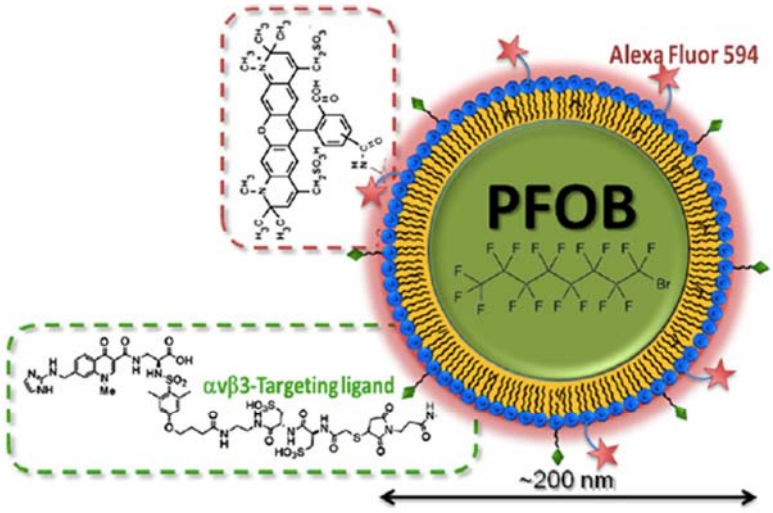

Figure 1. Diagrammatic illustration of perfluorocarbon nanoparticle structure with amb3-integrin targeting ligand and red fluorescent dye label [3].

Figure 2 shows results from combined proton/fluorine imaging in a rabbit model of angiogenesis performed on a clinical 3T scanner.

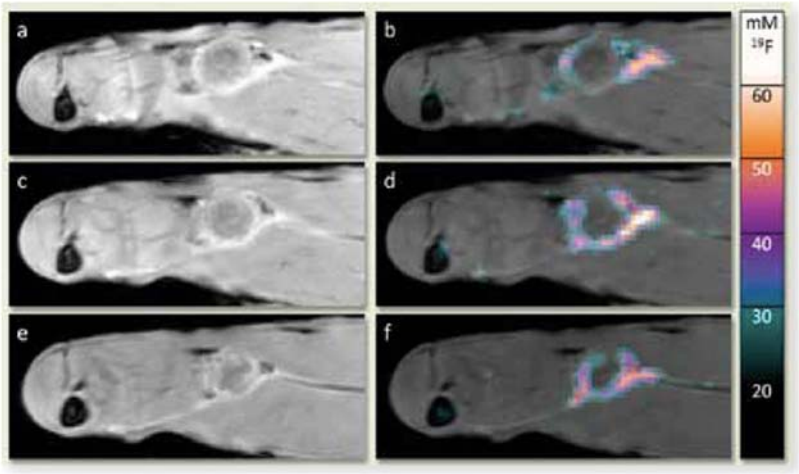

Figure 2 (reproduced from reference [4]). Quantification of $\alpha_v\beta_3$ -targeted nanoparticle (NP) concentrations via fluorine MRI on a Vx-2 tumor in the hind leg of a New Zealand White Rabbit. The milli-molar fluorine concentration from the NP at the target site (color scale 10–70 mM, right b,d,f) is superimposed with T1-weighted gradient echo images (left a,c,e) for anatomical co-localization in three selected image slices (out of 15). For an in-plane resolution of 2.2 mm and a slice thickness of 4 mm, the data acquisition was completed in 35 minutes. NP density can be derived from the fluorine concentrations and correlated with the degree of angiogenesis, which shows a heterogeneous pattern at the tumor rim as expected from tumor pathophysiology.

Active targeting of particulates can also be accompanied by external devices such as focused ultrasound which causes the nanoparticles to resonate and cavitate, thus releasing their "pay load". In addition to an imaging agent, the particles can also carry therapeutic drugs, thus enhancing the efficacy of therapy.

Phosphorus-31 endogenous metabolites

Phosphorus localized spectroscopy and imaging of endogenous metabolites can detect signals from inorganic phosphate (Pi), phosphocreatine (PCr), adenosine triphosphate (ATP), monoesters phosphoethanolamine (PE) and phosphocholine (PC), and diesters glycerophopshoethanolamine (GPE) and glycerophosphocholine (GPC). Either the absolute values, or ratios of these meatabolites can be used to access information about the cellular health of a particular tissue, in terms of the ATP levels for example, and parameters such as cellular pH can also be determined. Phosphocreatine recovery rates during exercise can be used to obtain an estimate of mitochondrial content and activity in healthy/diseased muscle tissue, and there are suggestions that a second Pi peak might be able to give similar information without requiring exercise [6].

The major application of ^{31}P CMI is in oncology. For example, many studies have shown an increase in phosphomonoesters in prostate tumour patients compared to healthy controls. At low magnetic fields it is difficult to determine the individual signals from monoesters PE and PC and diesters GPE and GPC. The ratios between these metabolite concentration,s as well as their absolute values, has shown been shown in many studies to be linked to malignancy in cell and tissue studies. Using a human 7 Tesla magnet the group of Scheenen [7] has provided a recent overview of the utility and sensitivity of phosphorus spectroscopic imaging in patients with prostate cancer. The authors conclude that there is significant overlap in the metabolite ratios between prostate cancer and normal-appearing tissue, but that distinctive values are obtained from patients with aggressive tumours.

Sodium-23 endogenous signals

^{23}Na is a quadrupolar nucleus with I=3/2. It has short T_1 values (<100 ms) and two components of transverse relaxation, one with a T_2 of ~25 ms and the other with a T_2 of ~2 ms. If sequences such as ultrashort echo time (UTE) or twisted projection imaging (TPI) [8] can be implemented, then the short T_1 allows extensive signal averaging within a reasonable imaging time in order to compensate for the relatively low sensitivity. Sodium MRI benefits especially from high field, since the relaxation times are not field dependent (unlike protons), and intracellular and extracellular components can potentially be separated using triple quantum filters [9] or different T_1 relaxation times.

The relationship between sodium MRI and molecular imaging is most relevant to studies of osteoarthritis (OA) and other related diseases [10]. The gold standard in OA diagnosis is still planar X-ray, but OA can only be diagnosed at a late stage when the only options are pain relief medication or joint replacement in the end

stage. There is a clear need for biomarkers and radiological imaging for early detection, diagnosis, and progression monitoring of OA with the goal of developing effective therapeutic drugs. As one of the building blocks of cartilage, sodium is strongly linked to the structural quality and mechanical properties of cartilage. Concentration changes of sodium within cartilage are sensitive to the very start of degradation, as shown in Figure 3.

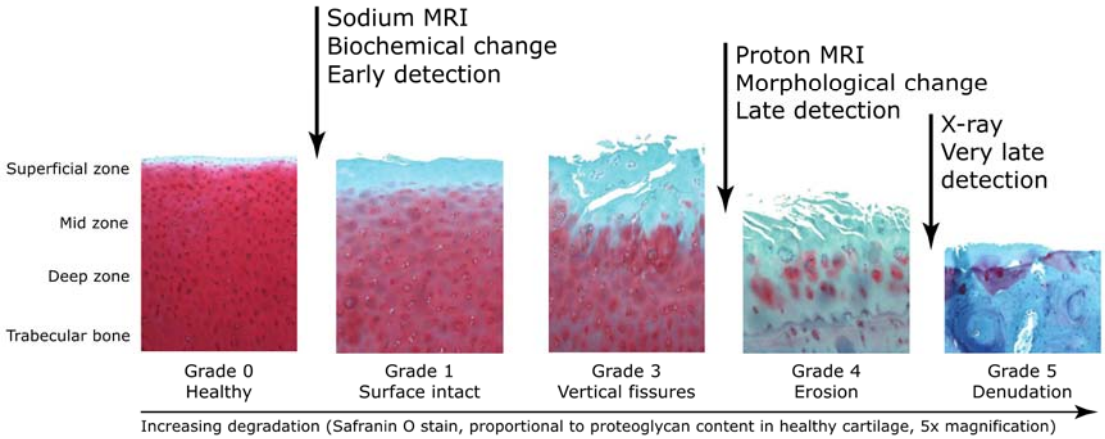

Figure 3. Histological timeline of cartilage degradationfrom healthy to fully denuded [11].

Figure 4 shows proton and sodium images of the human knee, acquired at 7 Tesla using a custom-built transmit/receive double-tuned birdcage volume coil in interleaved mode to increase the efficiency of data acquisition.

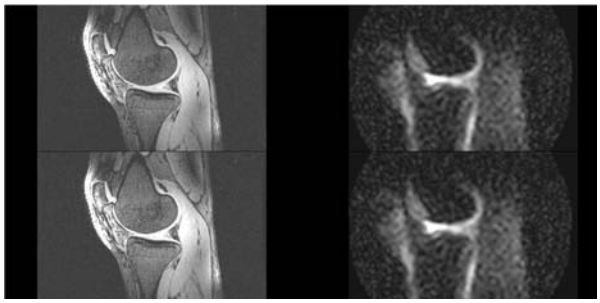

Figure 4. ^{1}H 3D gradient echo (FOV 220x220x141mm^3, 1mm isotropic resolution, TR 15ms, TE 2.5ms, tip angle 10^o, acquisition time 7m46s) and a ^{23}Na spiral gradient echo (FOV 220x220x153mm^3, 3x3x3mm^3 resolution, TR 100ms, TE 1ms, tip angle 90^o, acquisition time 10m24s). In the interleaved sequence five ^{1}H k-space lines are acquired in each ^{23}Na TR, resulting in a total scan duration for ^{1}H and ^{23}Na combined of 10m24s.

Carbon-13 exogenous agents: isotopic labeling and hyperpolarization

Carbon forms the backbone for all biological molecules, and given its very large chemical shift and sensitivity to small structural changes, it constitutes a very sensitive molecular imaging marker. However, as clear from Table 1, the NMR-active isotope ^{13}C is highly insensitive, mainly due to its low natural abundance. Apart from some lipid or glycogen studies, no practical experiments can be performed on natural abundance ^{13}C in the body. Up until a few years ago, the "solution" was to introduce ^{13}C labeled substrates into the body, in which isotopic enrichment of between 90 and 100% of ^{13}C was used. Such approaches are, however, extremely expensive to implement, and are essentially one-shot experiments. In 2008, signal enhancements up to 10,000 were demonstrated using the principle of dynamic nuclear polarization (DNP) [12] to produce ^{13}C in a hyperpolarized state, as shown in Figure 5. This has opened up a new frontier in ^{13}C-based molecular imaging. The afternoon session contains talks which deal with this topic in detail.

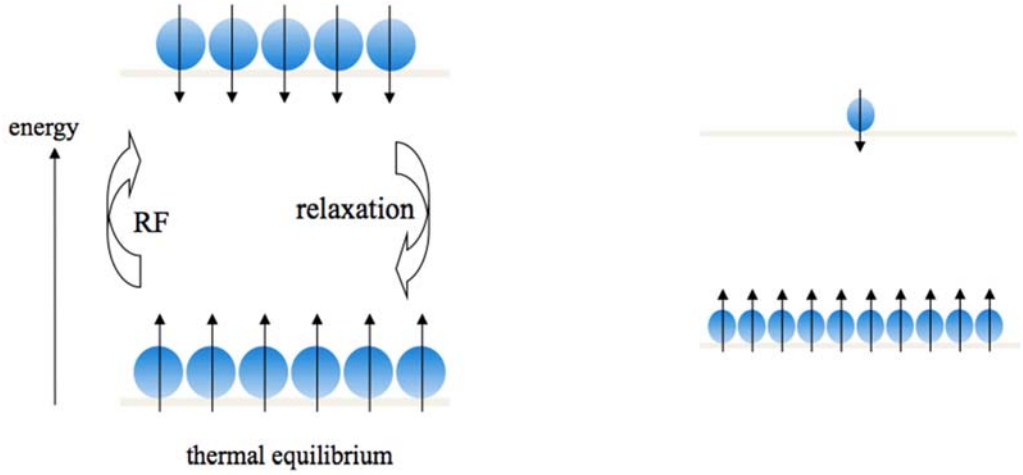

Figure 5. Hyperpolarization of nuclei (right) produces a highly non-Boltzmann distribution of parallel and anti-parallel energy states. The MR signal is proportional to the difference in occupation of the two levels, and thus is much enhanced by hyperpolarization.

Figure 6 shows the biochemical pathway by which detailed kinetic information and chemical fluxes can be derived from hyperpolarized ^{13}C spectroscopy after injection of a suitably hyperpolarized small molecule. One of the first in vivo examples is also shown, from a perfused mouse heart.

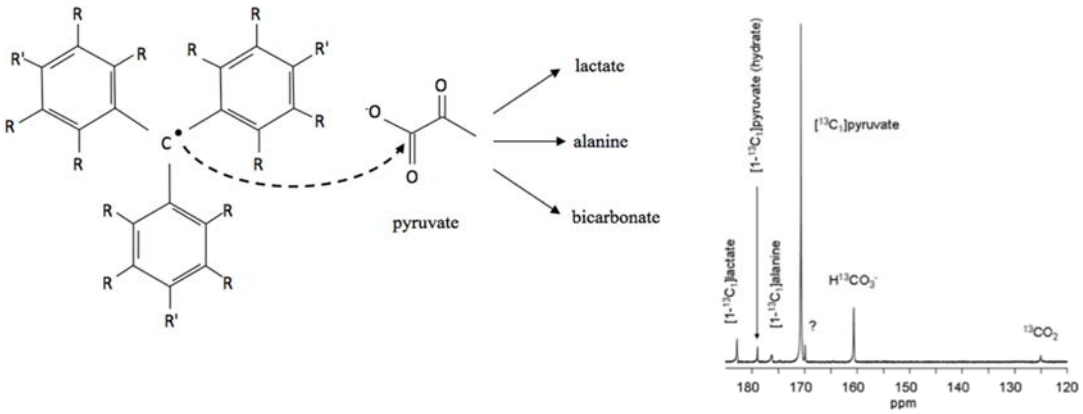

Figure 6. (left) Transfer of polarization from an electron of a stable trityl free radical to a carbon nucleus in pyruvate, which is further metabolized in vivo to give hyperpolarized lactate, alanine and bicarbonate. (right) ^{13}C NMR spectrum of a perfused mouse heart following injection of 2-mM hyperpolarized [1-13C pyruvate]. The spectrum is the sum of 70 scans [12].

Required hardware for non-proton MRI.

System requirements for performing non-proton MRI on either human or animal imaging systems consist of broadband RF amplifiers, a broadband receiver chain and appropriate multiple-tuned RF coils. The first two requirements are typically provided (or not) by the manufacturer, although there is a short-sighted trend towards proton-only systems. There are a myriad of designs for multiple-tuned transmit/receive, transmit-only/receive-only, and arrays of local receive coils (Mispelter). In general, there is a trade-off between system complexity and practical use, with the sensitivity of the proton channel suffering some reduction compared to a single-channel coil, while maintaining high sensitivity on the heteronuclear channel. Figure 7 shows one design of a double-tuned proton/phosphorus coils for imaging/spectroscopy of the human calf muscle.

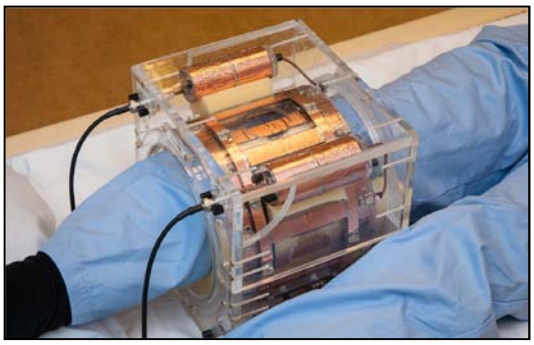

Figure 7. Photograph of an imbricated birdcage design for proton imaging and phosphorus spectroscopy of the calf muscle at 7 Tesla.

References.

[1] Webb AG, Wong M, Kolbeck KJ, et al. Sonochemically Produced Fluorocarbon Microspheres: A New Class of Magnetic Resonance Imaging Agent. *J.Magn.Reson. Imag.* **6**, 675-683 (1996).
[2] Schmieder AH, Winter PM, Williams TA et al. Molecular MR imaging of neovascular progression in the Vx2 tumor with $\alpha_v\beta_3$-targeted paramagnetic nanoparticles. *Radiology*, **268**, 470-480 (2013).
[3] Schmieder AH, Wang K, Zhang H et al. Characterization of early neovascular response to acute lung ischemia using simultaneous $^{19}F/^{1}H$ molecular imaging. *Angiogenesis*, 2013, doi 10.1007/s10456-013-9377-2.
[4] Caruthers SD, Winter PM, Wickline SA et al. MR molecular imaging of angiogenesis using targeted perfluorocarbon nanoparticles, *Medicamundi*, **43**, 5-13 (2010).
[5] Neubauer AM, Myerson J, Caruthers SD et al. Gadolinium-modulated 19F signals from perfluorocarbon nanoparticles as a new strategy for molecular imaging, *Magn.Reson.Med*. 60, 1066-1072 (2008).
[6] Kan HE, Klomp DWJ, Wong C et al. In vivo 31P MRS detection of an alkaline inorganic phosphate pool with short T1 in human resting skeletal muscle, *NMR Biomed.,* **23**, 995-1000 (2010).
[7] Lagemaat MW, Vos EK, Maas MC et al. Phosphorus magnetic resonance spectroscopic imaging at 7 T in patients with prostate cancer. *Investigative Radiology*, in press 2013.
[8] Boada FE, Gillen JS, Shen GX et al., "Fast three dimensional sodium imaging," *Magn Reson Med*. **37**, 706 (1997).
[9] R. Reddy, et al., "In vivo sodium multiple quantum spectroscopy of human articular cartilage," Magn Reson. Med. 38(2), 207 (1997).
[10] Borthakur A, Mellon AE, Niyogi S et al. Sodium and T1rho MRI for molecular and diagnostic imaging of articular cartilage. *NMR Biomed*, 19, 781–821, (2006).
[11] Pritzker K, Gay S, Jimenez K, et al. "Osteoarthritis cartilage histopathology: grading and staging1, 2," *Osteoarthr Cartilage*, vol. 14, no. 1, pp. 13–29, Jan. 2006.
[12] Ardenkjaer-Larsen JH, Fridlund B, Gram A. et al. Proc.Natl. Acad. Sci. U.S.A. 2003, 100 (18), 10158–10163.
[13] Merritt ME, Harrison C, Storey C et al;, Proc. Natl. Acad. Sci. U.S.A. 2007, 104 (50), 19773–19777.